



**HAL**  
open science

## A Structural Study of the Lyotropic Nematic Phase of Vanadium Pentoxide Gels

P. Davidson, C. Bourgaux, L. Schouffet, P. Sergot, C. Williams, J. Livage

► **To cite this version:**

P. Davidson, C. Bourgaux, L. Schouffet, P. Sergot, C. Williams, et al.. A Structural Study of the Lyotropic Nematic Phase of Vanadium Pentoxide Gels. *Journal de Physique II*, 1995, 5 (10), pp.1577-1596. 10.1051/jp2:1995200 . jpa-00248256

**HAL Id: jpa-00248256**

**<https://hal.science/jpa-00248256>**

Submitted on 4 Feb 2008

**HAL** is a multi-disciplinary open access archive for the deposit and dissemination of scientific research documents, whether they are published or not. The documents may come from teaching and research institutions in France or abroad, or from public or private research centers.

L'archive ouverte pluridisciplinaire **HAL**, est destinée au dépôt et à la diffusion de documents scientifiques de niveau recherche, publiés ou non, émanant des établissements d'enseignement et de recherche français ou étrangers, des laboratoires publics ou privés.

Classification

Physics Abstracts

61.10Lx — 61 30Eb — 82.70Kj

## A Structural Study of the Lyotropic Nematic Phase of Vanadium Pentoxide Gels

P. Davidson <sup>(1,2)</sup>, C. Bourgaux <sup>(3)</sup>, L. Schouffet <sup>(1)</sup>, P. Sergot <sup>(4)</sup>, C. Williams <sup>(3)</sup> and J. Livage <sup>(5)</sup>

<sup>(1)</sup> Laboratoire de Physique des Solides(\*), Bat. 510, Université Paris Sud, 91405 Orsay Cedex, France

<sup>(2)</sup> Materials Department, University of California, Santa Barbara, CA 93106, USA

<sup>(3)</sup> Laboratoire pour l'Utilisation du Rayonnement Electromagnétique(\*\*), Bat. 209D, Université Paris-Sud, 91405 Orsay Cedex, France

<sup>(4)</sup> Laboratoire de Physicochimie des Macromolécules(\*\*\*) , Ecole Supérieure de Physique et Chimie Industrielles de la Ville de Paris, 10 rue Vauquelin, 75231 Paris Cedex 05, France

<sup>(5)</sup> Laboratoire de Chimie de la Matière Condensée(\*\*\*\*), Université Pierre et Marie Curie, 4 Place Jussieu, 75252 Paris, France

(Received 20 April 1995, accepted 30 May 1995)

**Abstract.** — The aqueous suspensions of vanadium pentoxide ribbons are known to present a lyotropic nematic phase. The optical microscopy photographs of these suspensions in the gel and the sol states shown in this paper are indeed typical nematic textures. The biphasic (I/N) region shows tactoids which can be aligned by a magnetic field. Small angle X-ray scattering (SAXS) experiments were performed either on unoriented samples or on samples aligned by shear flow. The scattering is comparable to that of the other classic lyotropic nematic phases displayed by stiff organic rod-like particles. Scattering patterns give information on the transverse dimensions of the ribbons and on the average distance between them as a function of concentration. Estimates of the nematic order parameter were also obtained. Finally, the relevance of Onsager's model is discussed; the importance of the electrostatic interactions between ribbons in the onset of the nematic ordering of this system is stressed.

### Introduction

Inorganic lyotropic liquid crystals [1–8] are potentially interesting systems for applications because they may combine the fluidity and alignment properties of liquid crystals with the

---

(\*) URA 002

(\*\*) UMR 130

(\*\*\*) URA 278

(\*\*\*\*) URA 1466

electronic properties of inorganic materials, such as magnetism, conductivity, etc. In this respect, because of their more complex band structure, inorganic moieties containing transition metals [1,4,6,8] seem better candidates than the aluminosilicate-or aluminium hydroxide-based materials [2,3,5,7]. From a more fundamental point of view, inorganic lyotropic materials may also be good systems to test the different models of nematic ordering by X-ray scattering techniques, thanks to the large electronic contrast between the particles and the solvent. The vanadium pentoxide ( $V_2O_5$ ) gels [9], discovered in 1885 [10], represent such an example of a lyotropic nematic phase first recognized by Zocher in 1925 [1] and therefore sometimes called Zocher phases. In a recent letter [8], we have clearly demonstrated the liquid crystalline nature of this material and showed that its X-ray scattering pattern was quite comparable to those of the suspensions of Tobacco Mosaic Virus (TMV), a now classic example of lyotropic nematic phase [11]. From a different point of view,  $V_2O_5$  gels have raised interest as model colloids [12], and as intercalation compounds in chemistry [9]. Moreover, they are used as antistatic coatings in the photography industry [13], in electrochromic layers, as humidity sensors and as reversible cathodes for lithium batteries [9]. This article focusses essentially on the structure of the nematic phase, i.e., the determination of the transverse dimensions of the particles, of their average distance as a function of concentration, and of the nematic order parameter. The outline of this paper is the following : a first section recalls the synthesis and description of the  $V_2O_5$  gels. The second part is devoted to the different experimental set-ups. In the third part, we present on the one hand, the optical textures of these suspensions both in the nematic phase and in the biphasic region where Zocher's "tactoids" [1] are found, on the other hand the study by X-ray scattering of the molecular organization in the nematic phase, either in unoriented samples or in samples oriented by flow. Finally, the last section discusses the origin of the interactions leading to the nematic ordering.

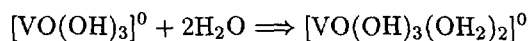
## 1. Chemical Synthesis and Description of Vanadium Pentoxide Gels

1.1. CHEMICAL SYNTHESIS. — Vanadium pentoxide gels are obtained via the acidification of aqueous solutions of vanadates [9]. A large variety of  $V^V$  species can be found in aqueous solutions depending mainly on vanadium concentration, pH and temperature. Monomeric orthovanadate species  $[VO_4]^{3-}$  are formed at high pH (pH  $\approx$  14). Upon acidification, protonation gives  $[H_nVO_4]^{(3-n)-}$  species. Condensation then occurs between hydroxylated precursors giving rise to polyanionic species such as pyrovanadate  $[V_2O_7]^{4-}$ , metavanadate  $[V_4O_{12}]^{4-}$  or decavanadate  $[V_{10}O_{28}]^{6-}$ .

Vanadium pentoxide gels were synthesized following procedures already described [9]. They are obtained free of foreign ions by an ion-exchange technique. An aqueous solution of sodium metavanadate  $NaVO_3$  ( $\approx$  1 mol  $l^{-1}$ ), is allowed to pass through a bed of a proton exchange resin (Dowex 50 W-X<sub>2</sub> 50-100 mesh). A yellow solution of vanadic acid is readily formed and fractionated in different vials. In some of these which present the right conditions of pH and concentration, this solution polymerizes slowly at room temperature giving rise to a dark red gel.

The formation of vanadium pentoxide gels  $V_2O_5$ ,  $n H_2O$  from neutral precursors  $[H_3VO_4]^0$  can be described as a three steps reaction as follows (Fig. 1):

i) An increase of coordination from 4 to 6, first occurs via the nucleophilic addition of two water molecules. This can be seen very easily as the color of the solution turns from white to yellow as soon as acidification is performed.



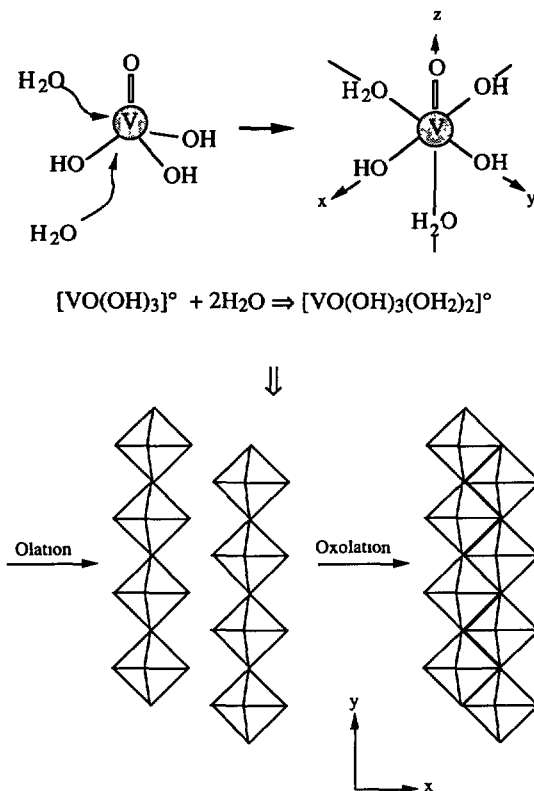
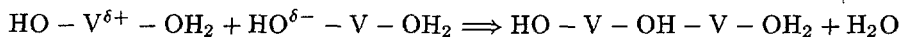


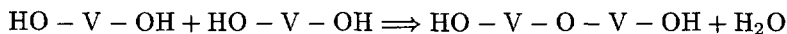
Fig. 1 — Formation of vanadium pentoxide gels from neutral precursors

This gives hexacoordinated species  $[\text{VO}(\text{OH})_3(\text{OH}_2)_2]^0$  in which one water molecule lies along the  $z$ -axis opposite to the short  $\text{V} = \text{O}$  double bond while the second one is in the equatorial plane opposite to one  $\text{OH}$  group. One  $\text{V}-\text{OH}_2$  and three  $\text{V}-\text{OH}$  bonds are formed in this plane so that  $x$ - and  $y$ -directions are not equivalent.

ii) Fast olation reactions then occur along the  $\text{HO}-\text{V}-\text{OH}_2$  direction giving rise to olated, corner-sharing polymers:

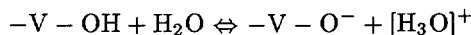


iii) Slower oxolation reactions then lead to the formation of edge sharing double chains:



This results in a ribbon-like structure made of vanadium pentoxide double chains in which  $[\text{VO}_6]$  octahedra share edges and corners (Fig. 1).

Once colloidal vanadium oxide species have been formed in the aqueous solution, water adsorption and dissociation occurs at the oxide-water interface giving rise to hydroxylated ribbons (Fig. 2). However because of the high positive charge of  $\text{V}^{\text{V}}$  ions, a strong electron transfer occurs within the  $\text{V} \leftarrow \text{OH}$  bond and surface  $\text{V}-\text{OH}$  groups exhibit acid properties:



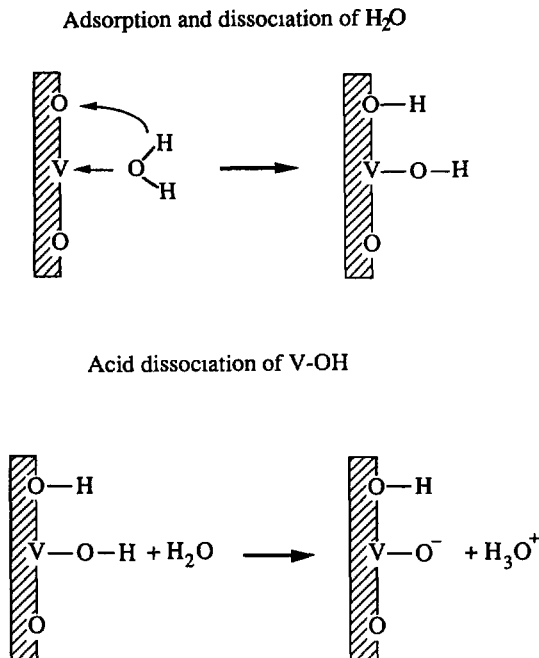


Fig. 2. — Adsorption and acid dissociation of water molecules at the  $\text{V}_2\text{O}_5\text{-H}_2\text{O}$  interface, leading to the formation of polyvanadic acid.

Vanadium oxide gels  $\text{V}_2\text{O}_5, n \text{H}_2\text{O}$  should therefore be described as polyvanadic acids  $\text{H}_x\text{V}_2\text{O}_5, n \text{H}_2\text{O}$  with a  $\text{pK}_a \approx 2$  for  $\text{V}_2\text{O}_5$  concentration of about  $1 \text{ mol l}^{-1}$ .

The acidic behaviour of vanadium oxide gels is responsible for their high proton conductivity,  $\sigma_{\text{H}} \approx 1 \Omega^{-1}\text{cm}^{-1}$  at room temperature. Moreover some vanadium reduction always occurs during the synthesis so that about 1% of the vanadium ions are in the reduced  $\text{V}^{4+}$  oxidation state. Some electronic conductivity can then be observed in dried xerogel ( $\text{V}_2\text{O}_5, 0.5 \text{H}_2\text{O}$ ) arising from a hopping process between  $\text{V}^{4+}$  and  $\text{V}^{5+}$  ions.  $\text{V}^{\text{V}}$  being easily reduced, special care should be taken when handling the samples in order to avoid further reduction that could lead to flocculation.

1.2. PHYSICAL DESCRIPTION. — Long, flat, more or less entangled  $\text{V}_2\text{O}_5$  ribbons are therefore formed and dispersed in the solvent. The typical dimensions of the ribbons, as estimated from electron microscopy images of dried samples [14], are a few 1000 Å long, about 100 Å wide and 10 Å thick (see Fig. 3). As for any polymer, the length (and, to a lesser extent, the width) has some degree of polydispersity which will depend on the polymerization conditions. Each ribbon seems to be made of about four identical threads  $\approx 25 \text{ Å}$  wide bonded side by side [14]. In contrast, the ribbons thickness is precisely determined by the size and association of the  $\text{V}_2\text{O}_5$  pyramids. The internal structure of the ribbons is closely related to that of orthorhombic  $\text{V}_2\text{O}_5$  [15]. They also are fairly rigid so that their typical persistence length is about 1000 Å. The vanadium pentoxide ribbons are negatively charged and bear a linear charge density of about  $0.5 - 1.5 \text{ e}^-/\text{Å}$ . These suspensions are of a dark red colour which only appears when polymerization takes place.

VANADIUM PENTOXIDE GEL - MAGNIFICATION 13,000

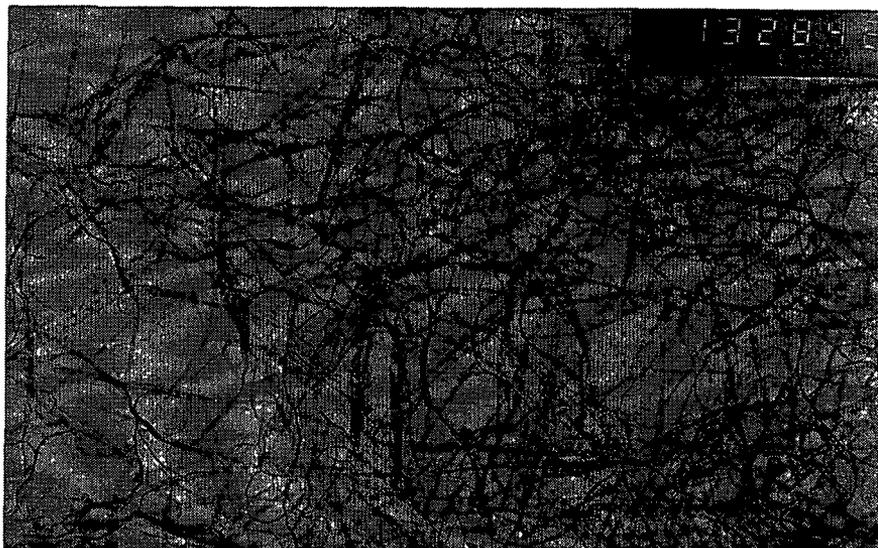


Fig 3. — Ribbons of  $V_2O_5$ .

The amount of water in the gels is determined from the weight loss observed when a sample is dried in an oven at  $500\text{ }^\circ\text{C}$ . Compositions will be expressed in  $\text{mol l}^{-1}$  of  $V_2O_5$  or, in an equivalent way, in terms of the number of  $H_2O$  molecules per  $V_2O_5$  unit:  $V_2O_5, n H_2O$ . In these suspensions, the water molecules seem to be of two kinds: on average, per  $V_2O_5$  unit, about two of them interact strongly with the ribbons whereas the others are more or less free. Indeed, slowly drying the suspensions at room temperature will result in the xerogel:  $V_2O_5, 1.8 H_2O$ . The remaining water molecules will only be eliminated by annealing at temperatures higher than  $250\text{ }^\circ\text{C}$ , a process which will result in the crystallization of orthorhombic  $V_2O_5$  at  $340\text{ }^\circ\text{C}$ .

Conversely, when dried around room temperature, the xerogels can be rehydrated. In the first stages, the swelling is discrete as a multilayer adsorption process takes place [9]. This regime is more characteristic of an intercalation compound rather than of a liquid crystal. Above  $n \approx 10$ , the swelling becomes continuous; it will be described in Section 3.2.

The rheological properties of  $V_2O_5$  suspensions have already been studied [9, 16]. At very low water content ( $n \leq 10$ ), the material is pasty as can be expected for a hydrated crystalline powder. The gels ( $10 \leq n \leq 250$ ) are clearly viscoelastic. A gel-sol transition then occurs at a concentration of about  $0.2\text{ mol l}^{-1}$ , that is  $V_2O_5, 250 H_2O$ . The sols are quite fluid but exhibit non-Newtonian viscosity effects (rheopexy). Altogether, the viscosity of the suspensions decreases regularly with increasing dilution.

Starting from a  $V_2O_5$  gel stock of a given concentration, one can change the composition either by slowly drying the material or diluting it with pure water. Either process allows us to obtain suspensions of different concentrations that all come from the same original batch and that have therefore identical chemical characteristics (polydispersity, impurities,  $V^{5+}/V^{4+}$  ratio, etc.).

## 2. Small Angle X-Ray Scattering Set-Ups

A first series of small angle X-ray scattering (SAXS) experiments has been carried out with a laboratory set-up, which has been already described in details elsewhere [17], using a rotating copper anode generator equipped with a microfocus. The beam is reflected from a cylindrical pyrolytic graphite monochromator and collimated with slits. The parallel beam delivers  $\approx 10^8$  photons per second in a  $0.5 \times 0.5 \text{ mm}^2$  cross section. The sample sits on a goniometer head and can be oriented and translated with respect to the beam. Vacuum flight tubes are used to prevent air-scattering. The scattered X-rays can be recorded either by a 2-dimensional detector or by a photographic film.

With this set-up, the samples were held in Lindeman glass capillary tubes of different diameters according to the  $\text{V}_2\text{O}_5$  concentration. Since the viscosity varies much with dilution, several techniques were used to fill the capillary tubes but, in all cases, we tried to obtain some flow alignment. Quite often, optical microscopy showed that highly oriented regions could indeed be produced this way. This was checked *in situ* by searching for oriented regions in the sample with the help of the 2-D detector. However, this method of alignment is not truly reliable and we therefore had to use another technique, namely a Couette shear cell.

A second series of SAXS experiments was conducted at the D22 and D24 stations of the LURE-DCI synchrotron radiation facility (Orsay, France). The basic design of these two instruments is similar [18] except for the monochromator. D22 has a double crystal (Si or Ge crystals), fixed exit monochromator giving a beam of narrow energy range tunable from 4 to 15 keV (3 Å to 0.8 Å). D24 uses a single bent Ge(111) crystal monochromator which provides a beam focused in the horizontal plane with a larger wavelength spread. D24 is preferred when high flux is required. In order to reduce parasitic scattering the beam path is kept under vacuum and antiparasitic slits are placed before the sample. The scattering profiles are recorded with a gas-filled (Ar-CO<sub>2</sub> or Xe-CO<sub>2</sub>), position sensitive detector or with imaging plates. The characteristics of these instruments widen the range of accessible scattering vector  $\mathbf{q}$  and obviate the need to correct the data for distortion due to the beam size. A good signal-to-noise ratio can be achieved. Furthermore, the high intensity allows measurements to be made with the Couette shear cell.

For static experiments, samples were held in flat Kelef cells with capton windows.

2.1. COUETTE SHEAR CELL. — The Couette shear cell is schematized in Figure 4. It will be described in more details in a forthcoming paper. As that of Safinya *et al.* [19], it has been specifically designed to carry out *in situ* X-ray scattering studies of complex fluids under shear flow. It consists of two concentric cylinders of outside radius 30 mm, made of polycarbonate. The size of the annular gap between them is 0.5 mm. The design of the cell allows one to rotate either the outer cylinder, with the inner one fixed, or the two cylinders to achieve small differential speed without instability. Each cylinder is driven by a motor associated to a tachometer forming a feedback loop which results in accurate speed control. This yields a constant shear rate  $\dot{\gamma}$  perpendicular to the cylinders. As the gap size is small compared to the radius of the cylinders we have:

$$\dot{\gamma} = R\Omega/d,$$

where  $d$  is the gap size,  $R$  the radius and  $\Omega$  the angular velocity of the cylinder. The highest velocity is 100 revolutions per minute.

The X-ray path is through the center of the cell so that the beam is parallel to the shear gradient.

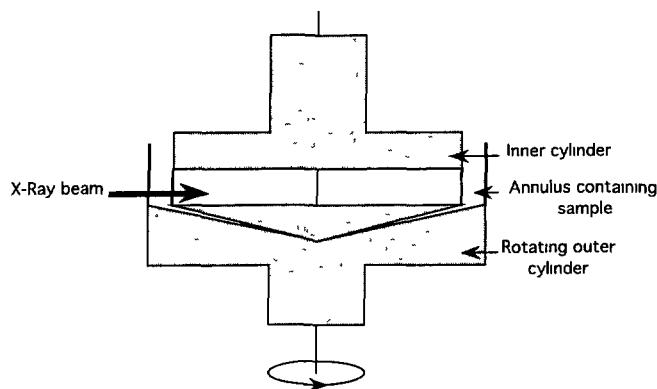


Fig 4 — Schematic drawing of the Couette shear cell.

2.2. DATA TREATMENT. — Before proceeding with the data analysis, the raw intensity data are corrected for sample transmission and thickness and normalized to the incident flux. The scattering curve of the water filled cell is then subtracted from the sample scattering curves. Intensities are thus comparable on a relative scale. Data are plotted as intensity *versus*  $q$  (the scattering vector modulus  $q = (4\pi/\lambda) \sin \theta$  where  $\theta$  is half the scattering angle).

### 3. Results and Interpretation

3.1. OPTICAL MICROSCOPY EXPERIMENTS. — For optical microscopy the samples were either squeezed between two glass slides or sealed in optical flat glass capillaries (microslides) of thicknesses 0.05 and 0.1 mm. Between crossed polarizers and in thin layers, the nematic gels usually display typical threaded textures (Fig. 5) and sometimes clear Schlieren textures with  $\pm 1/2$  disclination lines [20]. The nematic sols show fluid birefringent textures with slow spatial variations of the director (Fig. 6). The optical birefringence of a gel of concentration around  $0.3 \text{ mol l}^{-1}$  ( $\text{V}_2\text{O}_5$ ,  $200 \text{ H}_2\text{O}$ ) was previously estimated to be  $\Delta n \approx 0.01$  [8], a value slightly larger than those of other lyotropic nematic phases of stiff organic polymers.

The biphasic region around  $n \approx 500$ , between the isotropic and nematic phases (Fig. 7a) is quite interesting as it shows small nematic domains called “tactoids” (from the greek: “to assemble”) [1,21,22] These domains may take quite a long time to grow, typically a few weeks or even months, which explains why we did not observe them in our first experiments [8]. Inside a tactoid, the nematic phase may either appear uniformly oriented or clearly present topological defects. Note that the existence of tactoids in solutions of rigid rod organic polymers was also reported earlier [23]. More recently tactoids were studied by optical microscopy [7] in a dispersion of organophilic Boehmite rods. We have checked that the  $\text{V}_2\text{O}_5$  tactoids behave in exactly the same way (nucleation, shape, growth, coalescence, etc.).

Temperature has very little influence on the nematic phase: a sample of composition ( $\text{V}_2\text{O}_5$ ,  $180 \text{ H}_2\text{O}$ ) stays nematic up to more than  $200^\circ\text{C}$ , temperature at which it degrades. A sample of composition ( $\text{V}_2\text{O}_5$ ,  $400 \text{ H}_2\text{O}$ ) stays nematic up to  $150^\circ\text{C}$  where a reversible nematic/isotropic transition occurs. Around this temperature, a biphasic region is found where tactoids can be observed, these tactoids coalesce on cooling to form the nematic phase. In first approximation, the system is therefore athermal. A very schematic phase diagram is shown in Figure 8. The addition of a very small amount of a NaCl solution brings about the flocculation of the

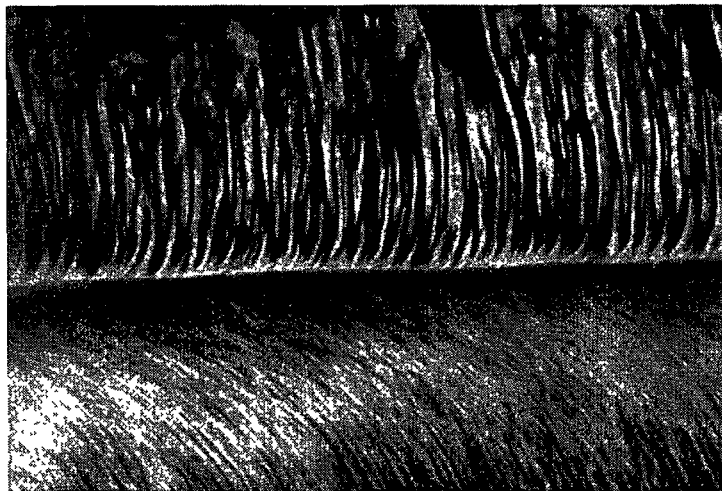


Fig. 5. — Optical texture in polarized light of a ( $V_2O_5$ , 180  $H_2O$ ) gel sample in a flat capillary (thickness 0.04 mm, magnification 400X). This texture is the result of the flow achieved on filling the capillary; on half of this image, a pattern very similar to the classical banded texture of polymers can be seen.

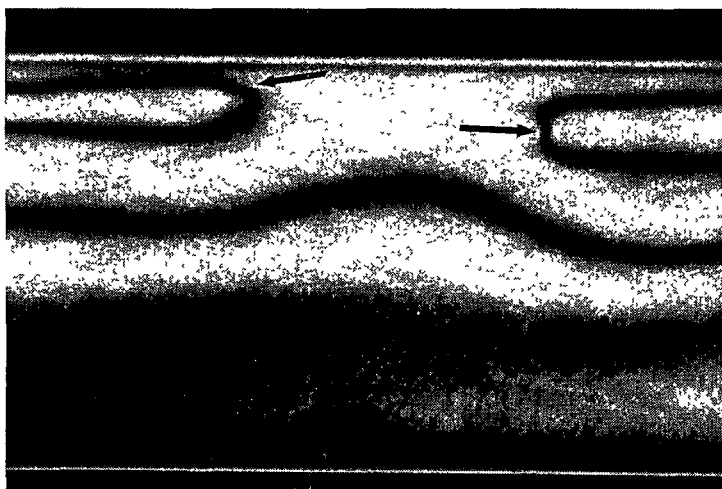


Fig. 6. — Optical texture in polarized light of a ( $V_2O_5$ , 400  $H_2O$ ) sol sample in a flat capillary (thickness 0.04 mm, magnification 100X). This is a typical schlieren texture with  $1/2$  disclination lines (arrows)

suspensions. At low water content, we could not detect a more ordered liquid crystalline phase such as a smectic one. (A hexagonal phase is not expected because of the highly biaxial geometry of the ribbons.) This might be due to the gel character of the suspensions which will prevent the reorganization of the ribbons on drying.

Applying an external magnetic field (1.5 T) did not produce any appreciable alignment of the nematic phase. However, in the biphasic region, the tactoids did rotate and align their

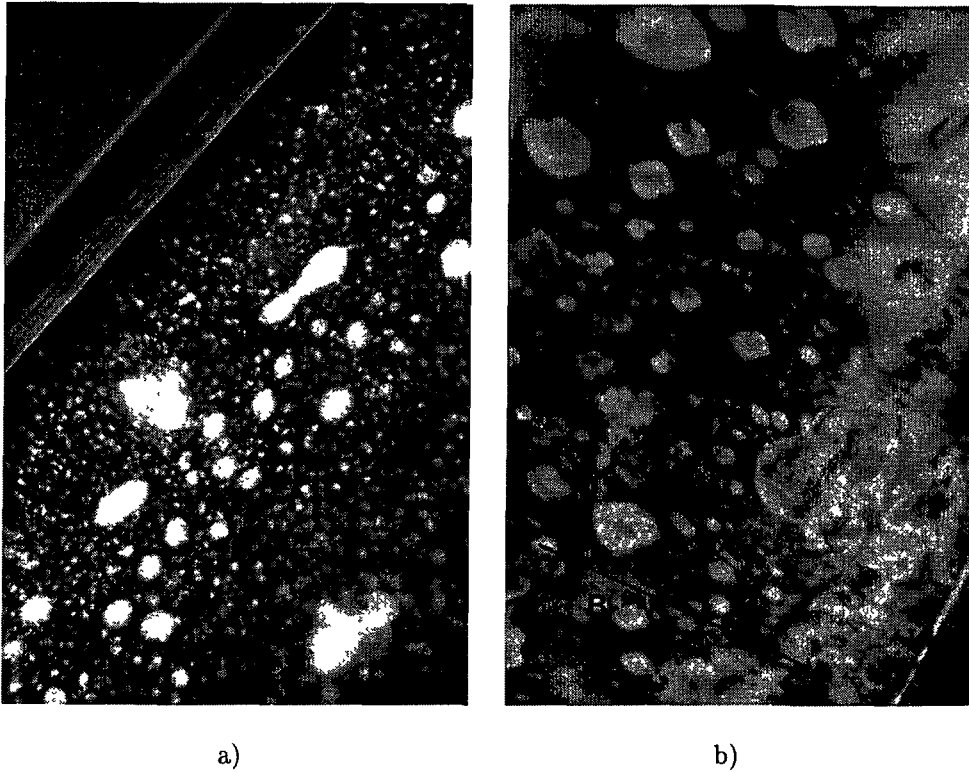


Fig. 7. — a) Polarized light micrograph of a ( $V_2O_5$ , 500  $H_2O$ ) sol sample showing phase separation after ageing for about a day. The yellow droplets are the nematic tactoids visible in the isotropic (dark) liquid. The arrows point to two coalescing tactoids (flat capillary of thickness 0.1 mm, magnification 250X); b) same conditions, the tactoids orient their long axis along the magnetic field direction represented by the arrow. (Applied field  $\approx 1.5$  T during 30 minutes).

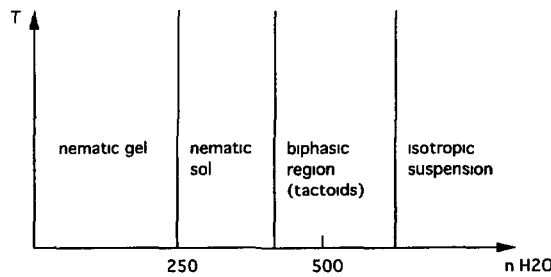


Fig. 8. — Schematic phase diagram of the ( $V_2O_5$ ,  $n H_2O$ ) system.

long axis along the field direction (Fig. 7b). More experiments using magnetic field and also involving the use of ferrofluids are presently under way.

In contrast, shear flow is an efficient way of aligning the suspensions, in both the gel and sol states. This can be checked either by optical microscopy or by X-ray scattering, as described

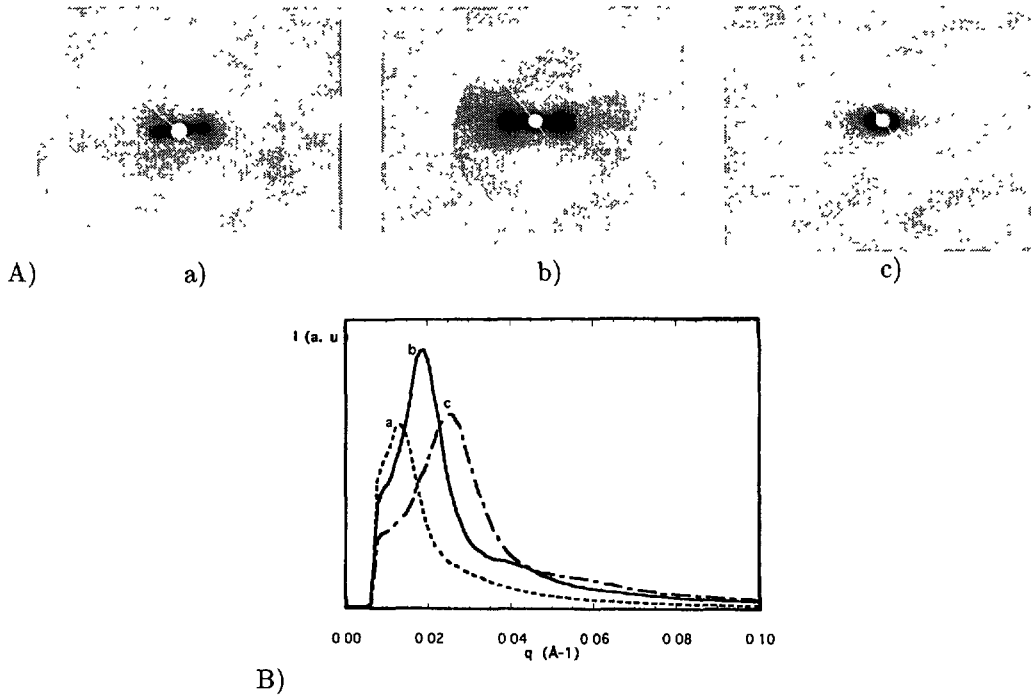


Fig 9. — A) SAXS patterns of oriented nematic ( $V_2O_5$ ,  $n$   $H_2O$ ) gels at different concentrations: a)  $n = 15$  (sample to photographic film distance: 28 cm); b)  $n = 26$  (sample to photographic film distance: 49 cm); c)  $n = 100$  (sample to photographic film distance: 49 cm). The capillary tube is vertical; B) SAXS patterns of nematic ( $V_2O_5$ ,  $nH_2O$ ) gels or sols at different concentrations: a)  $n = 350$ ; b)  $n = 220$ ; c)  $n = 140$ .

below in detail

3.2. SMALL ANGLE X-RAY SCATTERING EXPERIMENTS. — For an isotropic assembly of identical interacting particles the scattered intensity  $I(q)$  is the product of the shape factor  $P(q)$ , which describes the size and shape of a single particle, by the structure factor  $S(q)$ , which characterizes the spatial correlation between the particles. A complete structural description of the  $V_2O_5$  suspensions requires obtaining each function separately. As it is likely that  $V_2O_5$  ribbons are not altered upon dilution, measurements in very dilute isotropic suspensions will yield their shape factor  $P(q)$ . In contrast, interparticle interferences are expected to be important in concentrated systems and  $S(q)$  can be extracted from the total intensity.

Note that one advantage of working with inorganic suspensions, in comparison with other organic lyotropic systems [11, 24, 25], lies in their intrinsic strong scattering power due to the large contrast between the solvent and inorganic elements like vanadium. Hence high quality data can be obtained, even at low concentrations. As already discussed in a previous publication [8], SAXS patterns of oriented  $V_2O_5$  gels or sols in the nematic phase are quite similar to those of other lyotropic nematic phases of organic rigid rod polymers such as PBLG or Tobacco Mosaic Virus [24, 25]. One observes an anisotropic diffuse ring due to the lateral interferences among  $V_2O_5$  ribbons (Fig. 9a). The position in  $q$ -space of the diffuse ring maximum,  $q_{\max}$ , varies with water content and gives the lateral mean distance between the ribbons as  $d \approx 2\pi/q_{\max}$  for

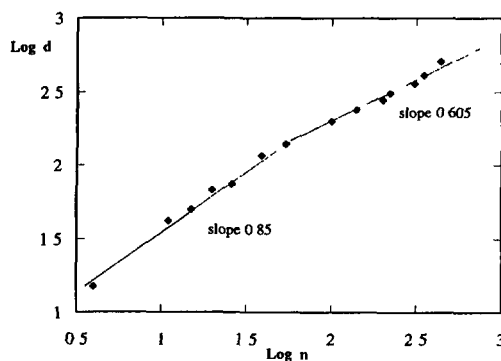


Fig. 10. — Variation of the mean lateral distance  $d$  between ribbons versus water content  $n$

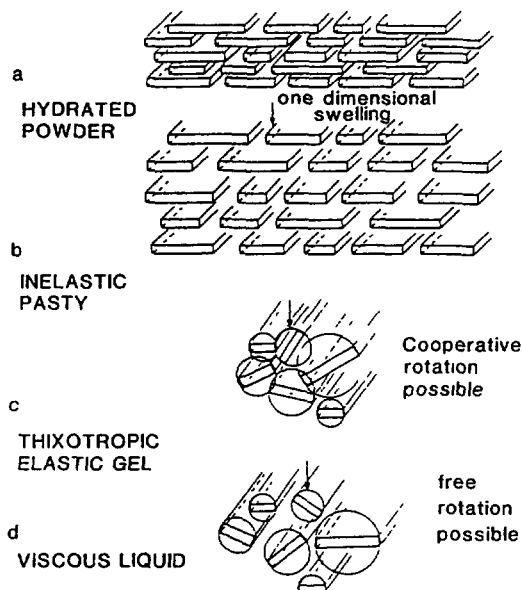


Fig 11 — Ribbons behaviour on dilution

the capillary tubes. This can be checked, by recording the wide angle scattering too since the anisotropy of the 001 and 002 intraribbon reflections also show the ribbons orientation axis. In most cases, this axis is, as expected, that of the capillary tube. However, the opposite orientation is also sometimes observed [8] (Due to a printing error, Figure 4 of reference [8] was not mounted properly and should be rotated by  $90^\circ$ ) which then implies a radial configuration of the director in the capillary tube.

Figure 9b shows some SAXS patterns of gels or suspensions at lower concentrations, recorded with a gas-filled detector. They are typical of all samples studied. The diffuse ring is actually observed in the whole nematic range ( $n \leq 500$ ). In contrast, the X-ray scattering patterns of dilute isotropic suspensions ( $n \geq 700$ ) do not show any small angle maximum in the observed

$q$  range: the isotropic scattering intensity decreases continuously with  $q$ . At intermediate concentrations ( $500 \leq n \leq 700$ ) a weak maximum is hardly detected at very small  $q$ . It should be emphasized here that this observation does not conflict with the isotropic nature of the suspension in this range: indeed the observed weak ring may arise from spatial correlations between ribbons without orientational order.

Figure 10 summarizes the measurements of the mean lateral distance  $d$  between ribbons *versus* water content  $n$ , obtained with the different X-ray set-ups. This figure can be compared to that of reference [26] which gathers characteristic sizes provided by various techniques on unoriented samples. Both sets of results are quite similar and show the same trends: when the number  $n$  of water molecules is small (i.e.,  $2 < n < 50$ ,  $10 \text{ \AA} < d < 100 \text{ \AA}$ ),  $d$  increases as  $n^{0.85}$ . A crossover takes place around  $n \approx 50$ ,  $d \approx 100 \text{ \AA}$  to another regime in which  $d$  increases as  $n^{0.60}$ . This behaviour was previously interpreted [26] in the following way: i) at low water content, the ribbons have their three main axes parallel on a local scale so that the swelling is essentially 1-dimensional (Fig. 11). An exponent of 1 is then expected, which is close to the observed 0.85. (It should be noted here that, though we do not have any evidence of it, we cannot actually rule out the possible existence of a biaxial nematic phase). This behaviour is reminiscent of that of intercalation compounds of which  $V_2O_5$  is an example. Extrapolation of this regime to  $n = 0$  gives the apparent ribbons thickness:  $e \approx 12.5 \text{ \AA}$  in good agreement with previous estimations [9, 14, 26]. ii) when the average distance between ribbons becomes comparable to their width ( $\approx 100 \text{ \AA}$ ), the ribbons are able to rotate around their long axis and the swelling becomes 2-dimensional as would be natural for a lyotropic nematic phase made of rigid rods. The expected exponent 1/2 is indeed close to the observed value of 0.6.

Information about the shape of non interacting particles can be obtained from the dependence of the scattered intensity on the scattering vector  $q$  [27]. In the so called "intermediate regime" for which at least one of the dimensions of the particle can be considered infinite compared to  $1/q$ , the scattered intensity should decay as  $I(q) \approx q^{-a}$ , with  $a = 1$  for an unoriented assembly of rods and  $a = 2$  for an unoriented assembly of flat particles. A typical log-log representation of the scattered intensity *versus* scattering vector in the case of a very dilute suspension ( $n = 750$ ) is presented in Figure 12a. One clearly sees two distinct regions: in the range  $0.02 \text{ \AA}^{-1} < q < 0.15 \text{ \AA}^{-1}$ ,  $I(q)$  decays as  $q^{-2}$  as expected from flat particles. At lower  $q$ 's,  $I(q)$  varies as  $q^{-0.65}$ . This crossover around  $q \sim 0.015 \sim 2\pi/400 \text{ \AA}^{-1}$  may be due to the fact that for smaller scattering vectors, the width of the ribbons cannot be considered infinite any more so that the ribbons look more like rods on this scale. However the  $q$  range where this variation is observed is too narrow to provide a precise value of the ribbons width.

More precisely, for flat homogeneous particles, the scattered intensity  $I(q)$  can be split into a factor of the area, proportional to  $q^{-2}$  and a "thickness factor"  $I_t(q)$ :

$$I(q) \propto \frac{1}{q^2} I_t(q)$$

This formula may be approximated by:

$$I(q) \propto \frac{1}{q^2} \exp\left(-\frac{q^2 t^2}{12}\right),$$

where  $t$  is the thickness of the particle.

By plotting  $\text{Log}(q^2 I(q))$  *versus*  $q^2$  in the range  $0.04 \text{ \AA}^{-1} < q < 0.25 \text{ \AA}^{-1}$ , the thickness of the ribbons can be deduced from the slope of the straight line obtained (Fig. 12b). A thickness of  $9 \pm 1 \text{ \AA}$  is found, in very good agreement with the other estimations.

Though it is difficult to obtain the ribbons width from the small angle scattering curves, we nevertheless can estimate it from the position of the diffuse ring at a given concentration [8]:

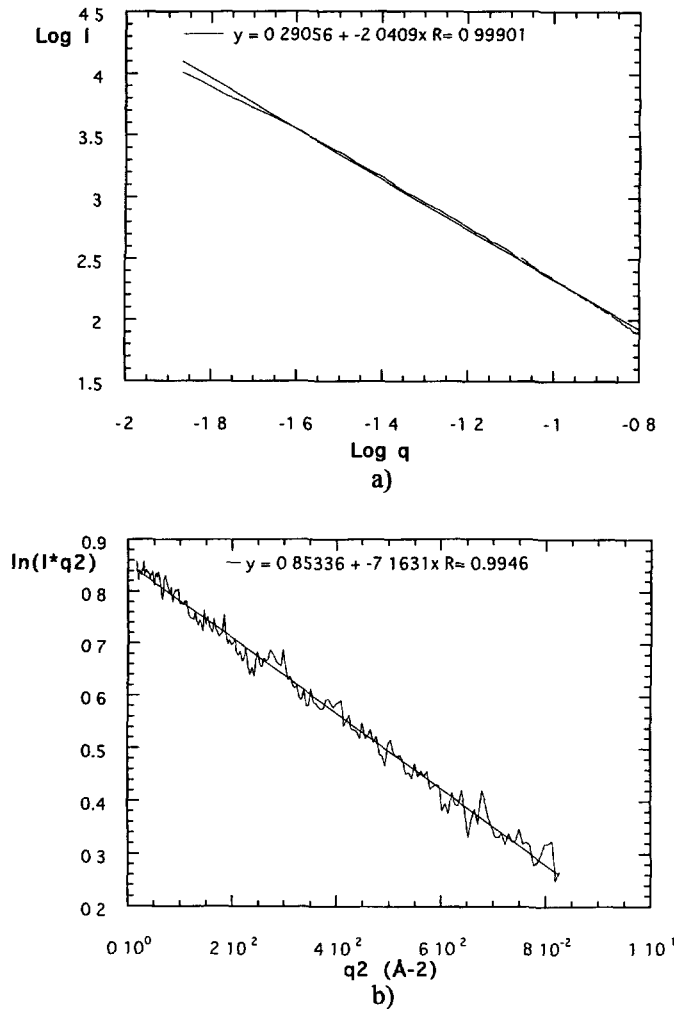


Fig. 12. — a) Variation of Log I as a function of Log q in the case of a dilute isotropic suspension ( $V_2O_5$ , 750  $H_2O$ ), b) variation of Log  $q^2/I(q)$  versus  $q^2$ .

a 1 mol  $l^{-1}$   $V_2O_5$  suspension displays a diffuse ring at  $q \approx 2\pi/160 \text{ \AA}^{-1}$ . The volume fraction of this suspension being  $\phi \approx 5\%$ , one can derive a cross-sectional area of about  $1300 \text{ \AA}^2$  for the ribbons. The thickness being ca.  $10 \text{ \AA}$ , this provides an estimation around  $130 \text{ \AA}$  for the ribbons width in good agreement with the previous ones. At this point, it should be stressed that the ribbons length lying in the range  $10^3$ – $10^4 \text{ \AA}$ , there is no much hope of deriving any information on this dimension from small angle X-ray scattering. Other techniques such as light scattering are needed to explore such a length scale.

In nematic suspensions it is still possible to determine the shape factor of the particles by neglecting the innermost part of the scattering curve dominated by the correlation between ribbons and by analysing the shape factor at higher  $q$ 's where the structure factor  $S(q)$  tends to its asymptotic value of 1. Figure 13 shows the log-log representation of the scattered intensity

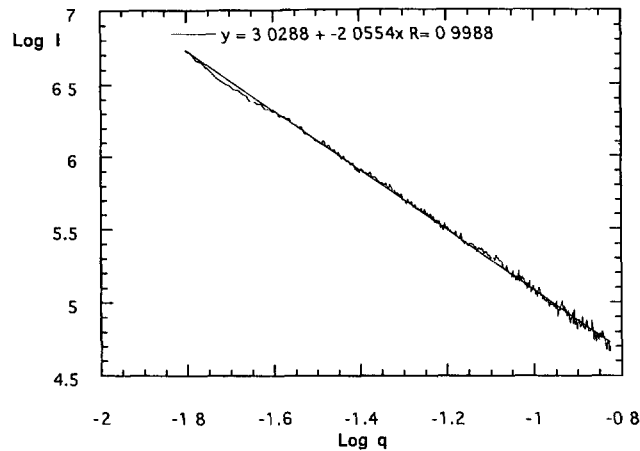


Fig. 13. — Variation of  $\text{Log } I$  versus  $\text{Log } d$  in the case of a nematic suspension ( $\text{V}_2\text{O}_5$ , 400  $\text{H}_2\text{O}$ ).

versus  $q$  in the case of a nematic suspension. It clearly shows that on a decade in  $q$ , the exponent  $a$  is very close to 2, a value typical of sheets. The same exponent is observed for all the nematic suspensions whatever the concentration. An exponent of 2 was already reported [28] in an earlier work but was supposed to be due to the existence of Gaussian random coils which are known to lead to the same exponent. Such an interpretation clearly conflicts with the observation of the nematic ordering of the ribbons. Moreover, electron microscopy images points to persistence lengths of the order of 1000 Å rather than values around 10 Å needed to observe a gaussian coil in this  $q$ -range.

Most probably, observing a coefficient close to 2 rather indicates that, in the range:

$$\frac{2\pi}{1000} \text{ \AA}^{-1} < \frac{2\pi}{100} \text{ \AA}^{-1} < q \frac{2\pi}{10} \text{ \AA}^{-1},$$

the ribbons can indeed be considered as platelets, as was correctly concluded in reference [26].

It should be noted here that the ribbons have the same form factor at all concentrations; diluting the suspensions does not alter the dimensions of the ribbons which were determined by the polymerization conditions.

Figure 14 shows the X-ray intensity scattered by samples sheared in the X-ray Couette shear cell (XCSC) and recorded on an Imaging plate. It is clear that, as intuitively expected, the ribbons are oriented parallel to the flow. Actually, this point is not so trivial: a nematic phase in a shear flow will orient at some finite angle  $\theta$  with the flow direction [20]. This angle depends on the ratio of the Leslie viscosity coefficients  $\gamma_1$  and  $\gamma_2$ . Only in the infinite chain limit does this ratio tend to unity so that  $\theta$  goes to zero and the nematic phase is oriented along the flow direction [29]. Thus this experimental observation of the nematic phase orientation under flow shows that the ribbons are indeed very anisotropic. Experiments were performed at different concentrations and shear rates. They provide a measure of a degree of orientation of the ribbons, the meaning of which is the following: if the sample were a single domain (the size of a nematic "domain" may be defined as an average distance between defects such as disclination lines), this degree of orientation would simply be the intrinsic nematic order parameter  $S$  [20].

Conversely, in the case of a distribution of domains (which is called the texture), the degree



Fig. 14. — SAXS pattern of the nematic ( $V_2O_5$ , 140  $H_2O$ ) gel sheared in the Couette cell at  $\gamma = 600 \text{ s}^{-1}$ .

of orientation thus measured only represents the nematic orientational distribution function inside a domain convoluted with the texture (This somewhat subtle point was discussed at length in reference [17]). The procedure used to measure the nematic order parameter from the lateral intermolecular interferences is now quite well documented [30]. By considering the scattering units as cylindrical uniform rods, Leadbetter *et al.* [30a,b] derived a relation between the polar intensity distribution (Fig. 15) and the nematic orientational distribution function. Later, Paranjpe and Kelkar [30c,d] showed that this relation was extremely simplified when assuming a Maier-Saupe distribution; the scattered intensity should be fitted to the following

simple form:  $I(\theta) = \frac{e^{m \cos^2 \theta} \sqrt{\pi}}{\sqrt{m} Z \cos \theta} \frac{\text{erf}(\sqrt{m} \cos \theta)}{2}$ , where  $Z$  is a normalization constant and

$m$  represents the strength of the nematic interaction (in units of  $k_B T$ ). The nematic order parameter is finally obtained from the value of  $m$ . A detailed discussion of the validity of this procedure can be found in reference [30e]. Figure 15 shows that, in our case, the scattered intensity is indeed well described by this simple form, although the ribbons can hardly be considered cylindrical and furthermore we do not always have a single domain. This fairly good description of the data is probably ensured by the large disorder typical of the nematic phase. Consequently, the biaxial local order is probably weak; indeed, we actually measured a swelling exponent of 0.85 instead of one. Another consequence is that taking averages either on the scale of the sample or on that of a nematic domain does not essentially change the form of the distribution. This point is related to the "cluster" assumption underlying the derivation of the above integral formula [30a,b].

In the absence of shear, the scattering is isotropic whatever the concentration, even in the case of nematic suspensions. This means that the texture is isotropic. As soon as a very low shear rate (of the order of  $6 \text{ s}^{-1}$ ) is applied to a nematic gel a very strong scattering anisotropy is observed (see Table I). Increasing the shear rate does not result in a significant increase of anisotropy. Stopping the shear and letting the sample relax does not decrease the order parameter at least for short times of the order of tens of minutes. This behaviour can be understood by considering that even a very small shear is sufficient to align the nematic gel so that a stable nematic gel single domain is produced. In this case, the nematic order

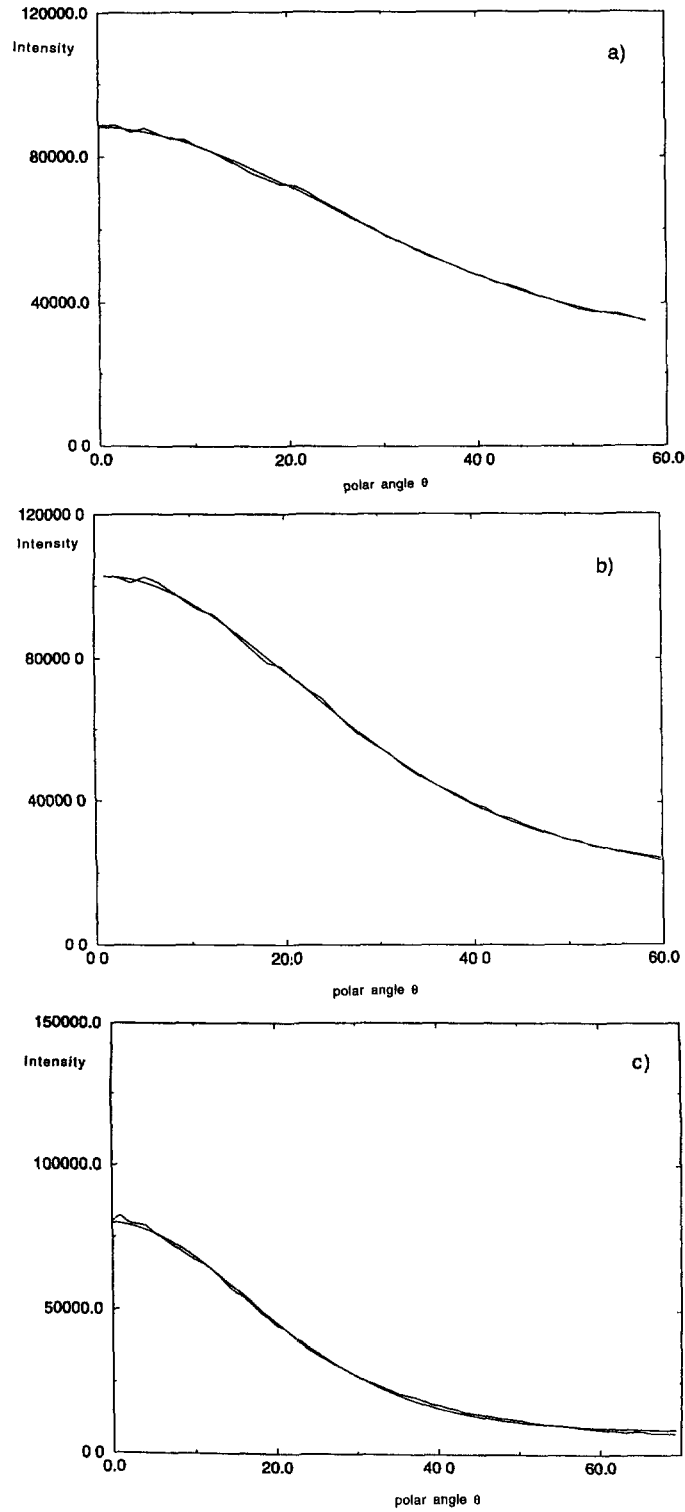


Fig. 15 — Scattered intensity  $I$  versus polar angle  $\theta$  a) ( $V_2O_5$ , 350  $H_2O$ )  $\gamma = 6 \text{ s}^{-1}$ , b) ( $V_2O_5$ , 350  $H_2O$ );  $\gamma = 600 \text{ s}^{-1}$ ; c) ( $V_2O_5$ , 220  $H_2O$ );  $\gamma = 600 \text{ s}^{-1}$

Table I. — *Orientation degree versus shear rate for different concentrations.  $m$  is the Maier-Saupe parameter,  $S$  is the apparent nematic order parameter (error bars  $\approx 5\%$ ) as explained in the text. a) sample aligned by flow in a capillary tube and recorded on the rotating anode set-up; b) no detectable effect; c) detectable but not measurable effect.*

$n$	$\gamma$ ( $s^{-1}$ )	$m$	$S$	
60	-		0.75	(a)
140	6	5.43	0.67	
140	60	5.48	0.67	
140	600	4.18	0.66	
220	6	4.0	0.63	
220	60	5.50	0.68	
220	600	2.55	0.69	
350	6	2.57	0.37	
350	60	3.64	0.52	
350	600	3.94	0.55	
440	6	2.17	0.32	
440	60	2.83	0.42	
440	600	3.22	0.47	
680	6	-	-	
680	60	-	-	(c)
680	600	0.95	0.15	

parameter estimated by the procedure mentioned above can be thought of as the intrinsic nematic order parameter. In contrast, in the case of the nematic sols, Table I shows that the apparent nematic order parameter estimated this way depends strongly on the shear rate. This dependence is probably too strong to be intrinsic. More probably, the maximum shear was not strong enough to provide a nematic sol single domain and the nematic order parameter only represents the convolution of the intrinsic nematic order parameter with the remaining texture distribution. Shearing an isotropic solution does give rise to an appreciable orientation at high shear rates ( $600 s^{-1}$ ). In that case, the order parameter obtained is intrinsic since there cannot exist any nematic domain. The orientation observed is quite similar to flow birefringence in optics [31] and its magnitude is quite appreciable (Tab. I). This observation also confirms that the isotropic phase is really constituted by elongated objects in solution. Suppressing the shear results in a rapid loss of orientation which is typical of the isotropic liquid nature of the phase.

#### 4. Discussion

This part essentially focusses on the statistical physics models which may be used to describe the nature of the interactions between the  $V_2O_5$  particles and the appearance of the nematic ordering. The background of this discussion is provided by the recent comprehensive review article by Vroege and Lekkerkerker [32] about lyotropic nematic liquid crystals and also by the article of Fraden, Maret and Caspar on the nematic phase of TMV [11].

The first observation that could give a clue to a theoretical description is that the system seems to be athermal. This feature is characteristic of Onsager's model [33] in which the

particles only interact through excluded volume interactions (The isotropic/nematic transition is here driven by a net increase of translational entropy versus orientational entropy of the rods). Onsager's model is quantitatively valid only for cylindrical rods of very high aspect ratio  $L/D \approx 100$  where  $L$  is the rod length and  $D$  its diameter.  $V_2O_5$  ribbons are certainly not cylindrical but nonetheless one can at least try to apply the available models by considering the diameter  $D_{eq}$  of an equivalent cylinder of the same cross section as that of the actual  $V_2O_5$  ribbon ( $\frac{\pi}{4}D_{eq}^2 \approx 10 \times 100 \text{ \AA}^2$ ,  $D_{eq} \approx 36 \text{ \AA}$ ). This bold step can be justified by the fact that the swelling was shown to be 2-dimensional at the nematic/isotropic transition because the ribbons rotate around their main axis. Then, we can estimate a very large aspect ratio:  $\frac{L}{D_{eq}} \approx \frac{3000}{36}$  close enough to 100 for Onsager's theory to be quantitatively valid. In order to check this assumption, we calculate the dimensionless particle concentration at the transition:  $V_2O_5$ , 500  $H_2O$  corresponds to a molarity of  $0.12 \text{ mol l}^{-1}$ , the molar weight of  $V_2O_5$  being 182 g and its density 3.38, the volume fraction of the rods is  $\phi \approx 6.5 \times 10^{-3}$ , which is very low. The dimensionless particle concentration is then given by:  $c = \frac{L}{D_{eq}}\phi \approx 0.55$  (number density  $\rho \approx 2.2 \times 10^{21} \text{ m}^{-3}$ ) almost an order of magnitude smaller than the predictions of Onsager's model (Onsager's model predicts:  $c_i \approx 3.3$ ,  $c_a \approx 4.2$ ,  $S \approx 0.8$ ). At this point, the observation that a small addition of brine strongly destabilizes the nematic phase points to the importance of electrostatic interactions. Indeed, the ribbons bear a quite appreciable linear charge density ( $\nu \approx 0.5 - 1.5 \text{ e}^-/\text{\AA}$ ) and these interactions are known to play an important role in the existence of the nematic phase of TMV, for instance. These electrostatic effects were incorporated in the theory by Stroobants *et al.* [34] and applied also to the case of the TMV suspensions [11]. This results into two effects: on the one hand, the diameter of the object should be replaced by some effective diameter  $D_{eff}$  which depends on the linear charge density and the Debye length of the system. This stabilizes the nematic phase at lower dimensionless particle concentration. On the other hand, a "twisting effect" also occurs because two charged rods tend to orient themselves perpendicularly and this destabilizes the nematic phase. In our case, we estimate Debye's length to be  $\kappa^{-1} \approx 40 \text{ \AA}$  and  $\nu$  to be  $0.5 - 1.5 \text{ e}^-/\text{\AA}$ . From these values, Table II of reference [32] allows to estimate the effective diameter:  $D_{eff} \approx 10D_{eq} \approx 350 \text{ \AA}$  and the "twist parameter" is at most.  $h \approx 0.2$ . In another crude approximation, we can neglect the influence of the twist effect because it affects the transition concentration by about 10% only (see Fig. 4 of Ref. [32]). Then we recalculate the transition concentration using Onsager's model with the effective diameter:  $c = \frac{1}{4}\pi L^2 D_{eff} \rho \approx 5.4$ , which is now of the correct order of magnitude when considering all the approximations and simplifications made in this reasoning. However, the effective aspect ratio  $L/D_{eff}$  is now around 10 which is too low for Onsager's model to be quantitatively valid. Nevertheless, this indeed shows us the important role played by the electrostatic interactions in the onset of nematic ordering in this system. Other experiments in which the ionic strength of the solvent is systematically varied, are clearly needed to better assess this point

Another discrepancy between model and experiment is going to point to another feature of this system which was not considered so far in this discussion: Onsager's and other related models predict very large order parameters ( $S \approx 0.7 - 0.8$ ) at the  $I/N$  transition for aspect ratios of 10 and more. Though we were not able to properly measure the order parameter at the transition by lack of a true single domain, our order parameter estimations in the gel state, where we believe that the shear produces a single domain, indicate  $S \approx 0.6 - 0.7$  well below the expected values. Moreover, the evolution of  $S$  with the dimensionless concentration does not follow the Onsager prediction  $S \approx 1 - 3\pi/4c^2$ . This may come from the fact that we

have neglected the ribbons flexibility. Electron microscopy images do show that the persistence length is in the range of  $\approx 1000 \text{ \AA}$ , i.e., smaller than the overall ribbon length  $L \approx 3000 \text{ \AA}$ . A worm-like chain description may therefore be more appropriate and will result in decreasing the order parameter at the transition.

To proceed further in this analysis, more experimental studies will be needed for instance by light scattering in order to measure the average length and persistence length of the ribbons. Another important but unknown factor is the polydispersity as the longer chains will apparently decrease the transition concentration and the shorter chains will decrease the saturated order parameter.

Finally, let us briefly mention that a very similar discussion can also be made about another inorganic compound [6], namely  $\text{Li}_2\text{Mo}_6\text{Se}_6$ . This material made of long cylindrical rods presents a lyotropic nematic phase down to  $\phi \approx 7 \times 10^{-3}$ ,  $c \approx 0.7$ . Such a low value can also be explained by incorporating electrostatic interactions into Onsager's model which provides the correct order of magnitude for the transition concentration, just like the  $\text{V}_2\text{O}_5$  suspensions.

### Acknowledgments

It is a pleasure to thank P. Batail, J.C. Gabriel, P. Pieranski and J. Prost for enlightening discussions and M. Clerc and A.M. Levelut for help with some of the synchrotron experiments. P. Davidson gratefully acknowledges support from a NATO research fellowship. The shear flow cell was built with the help of CPR CNRS PIRMAT "Polymères hydrosolubles associatifs".

### References

- [1] Zocher H., *Z. Anorg. Allg. Chem.* **147** (1925) 91
- [2] Emerson W.W., *Nature* **178** (1956) 1248.
- [3] Zocher H. and Torok C., *Kolloid Z.* **170** (1960) 140
- [4] Maeda Y. and Hachisu S., *Colloids Surf.* **6** (1983) 1
- [5] Kajiwara K., Donkai N., Hiragi Y. and Inagaki H., *Makromol. Chem.* **187** (1986) 2883.
- [6] (a) Davidson P., Gabriel J.C., Levelut A.M. and Batail P., *Europhys. Lett.* **21** (1993) 317; (b) Davidson P., Gabriel J.C., Levelut A.M. and Batail P., *Adv. Mater. Res. News* **5** (1993) 665.
- [7] Buining P.A. and Lekkerkerker H.N.W., *J. Phys. Chem.* **97** (1993) 11510.
- [8] Davidson P., Garreau A. and Livage J., *Liq. Cryst.* **16** (1994) 905.
- [9] For a recent review of the general properties of  $\text{V}_2\text{O}_5$  gels, see: Livage J., *Chem. Mater.* **3** (1991) 578 and references therein.
- [10] Ditte A., *C.R. Acad. Sci. Paris* **101** (1885) 698.
- [11] Fraden S., Maret G. and Caspar D.L.D., *Phys. Rev. E* **48** (1993) 2816 and references therein.
- [12] (a) Errera J., Overbeek J. and Sack H., *J. Chim. Phys.* **32** (1935) 681; (b) Donnet J.B., Zbinden H., Benoit H., Daume M., Dubois N., Pouyet J., Scheibling G. and Vallet G., *J. Chim. Phys.* **47** (1950) 52; (c) Donnet J.B., *J. Chim. Phys.* **50** (1953) 291.
- [13] (a) Guestaux C., August 1971, French patent 2 153 123; (b) Guestaux C., Leaute J., Virey C. and Vial J., April 1972, US patent 3 658 573.
- [14] Legendre J.J. and Livage J., *J. Colloids Interface Sci.* **94** (1982) 75.
- [15] Bachmann H.G., Ahmed F.R. and Barnes W.H., *Z. Kristall.* **115** (1961) 110.
- [16] Bailey J.K. et al., *Mat. Res. Soc. Symp. Proc.* **180** (1990) 759
- [17] Degert C., Davidson P., Megtert S., Petermann D. and Mauzac M., *Liq. Cryst.* **12** (1992) 779.

- [18] See for instance: Dubuisson J.M., Dauvergne J.M., Depautex C., Vachette P. and Williams C.E., *Nucl. Instr. Meth. Phys. Res.* **A246** (1986) 636.
- [19] Safinya C.R., Sirota E.B. and Plano R.J., *Phys. Rev. Lett.* **66** (1991) 1986.
- [20] For general properties of liquid crystals, see for instance. de Gennes P.-G., *The Physics of Liquid Crystals* (Clarendon Press, Oxford, 1979)
- [21] Wojtowicz W., Ph. D. Thesis, Wayne State University, Detroit, USA (1952).
- [22] Heller W., *Polymer Colloids*, Vol. II, E. Fitch, Ed. (Plenum Press, 1980) p. 153.
- [23] Panar M. and Beste L.F., *Macromol.* **10** (1977) 1401.
- [24] Oldenburg R., Wen X., Meyer R.B. and Caspar D.L.D., *Phys Rev Lett.* **61** (1988) 1851.
- [25] Ao X., Wen X. and Meyer R.B., *Physica A* **176** (1991) 63.
- [26] Baffier N., Aldebert P., Livage J. and Haesslin H.W., *J Colloid Interface Sci.* **141** (1991) 467.
- [27] (a) Guimer A. and Fournet G., *Small Angle Scattering of X-Rays* (J. Wiley & Sons, New York, 1955); (b) Glatter O. and Kratky O., *Small Angle X-Ray Scattering* (Academic Press, New York, 1982).
- [28] Kamiyama T., Itoh T., Suzuki K., *J. Non-Cryst Solids* **100** (1988) 466.
- [29] Meyer R.B., *Polymer Liquid Crystals*, A. Ciferri, W.R. Krigbaum and R.B. Meyer, Eds. (Academic Press, 1982) Chapter 6.
- [30] (a) Leadbetter A.J. and Norris E.K., *Molec. Phys.* **38** (1979) 669, (b) Leadbetter A.J. and Wrighton P.G., *J. Phys. France* **40**(1979) C3-324; (c) Paranjpe A.S. and Kelkar V.K., *Mol. Cryst. Liq. Cryst. Lett.* **102** (1984) 289; (d) Kelkar V.K. and Paranjpe A.S., *Mol. Cryst. Liq. Cryst. Lett.* **4** (1987) 139; (e) Davidson P., Petermann D. and Levelut A.M., *J Phys. II France* **5** (1995) 113.
- [31] (a) Doi M. and Edwards S.F., *The Theory of Polymer Dynamics* (Clarendon Press, Oxford, 1986); (b) Janeschitz-Kriegl H., *Adv. Polymer. Sci.* **6** (1969) 170.
- [32] Vroege G.J. and Lekkerkerker H.N.W., *Rep. Prog. Phys.* **55** (1992) 1241
- [33] Onsager L., *Ann N.Y. Acad. Sci.* **51** (1949) 627.
- [34] Stroobants A., Lekkerkerker H.N.W. and Odijk Th., *Macromol.* **19** (1986) 2232.